Modelling and Optimum Redesign of Reluctance Magnetic Leadscrew

E. K. Joergensen, F. E. Jensen, K. E. B. Andersen, M. Titel

Department of Materials and Production, Aalborg University
Fibigerstraede 16, DK-9220 Aalborg East, Denmark
Email: {ejarge18, feje18, keba18, mtitel21}@student.aau.dk,
Web page: http://www.mechman.mp.aau.dk/

Abstract

In this project a magnetic linear actuator (MLA) is investigated for the purpose of replacing a mechanical linear actuator (MeLA). The MeLA is a Linak LN36 provided by Linak and compared to a prototype of a MLA, which is also provided by Aalborg University. Several experiments have been conducted in order to determine the magnetic field and the force-displacement curve of the MLA. The results of these experiments serve as basis for the validation of the finite element model, which is used for optimizing the design of the MLA. Three optimization cases are set up to investigate different optimum designs. These designs are compared to each other and to the MeLA, and it is found that the MeLA can be replaced by MLA concepts in regards to stall force.

Keywords: Reluctance Magnetic Leadscrew, Mechanical Leadscrew, Magnetic Linear Actuator, Mechanical Linear Actuator

1. Introduction

Linear actuators are widely used in industrial applications, office environments and consumer products. Traditionally, these types of linear actuators work with the mechanical nut and leadscrew principle in which friction and wear is inevitable. Furthermore, the leadscrew is not suited for food-grade environments requiring extensive cleaning. As an alternative, the MLA concept has extended lifetime with reduced wear and high efficiency. However, they are not widely used. In this paper, a general design of reluctance-based MLAs will be investigated for the purpose of replacing MeLA.

The project takes offset in a well known MeLA provided by Linak from which a set of specifications is established. These are used to ensure a ground for comparison between the MeLA and MLA. The prototype MLA is therefore similarly investigated with experiments and models to determine its relevant performance specifications. Based on the findings regarding the MLA, an optimization is made to find the optimum redesign of the MLA.

Three cases are established for investigation of optimum design:

1.1 Case 1

It is investigated how large of a stall force the MLA can achieve, while abiding by the same dimensional constraints as the MeLA. The intention is to enable a direct replacement of the MeLA with the MLA without any major changes in implementation.

1.2 Case 2

A similar approach as case 1 where the MLA should replace the MeLA directly is used here. The objective for this case is to ensure that the MLA force matches the MeLA force exactly while keeping the volume at a minimum, as opposed to case 1 where the force is maximized within dimensional constraints. The dimensional constraints are removed in this case.

1.3 Case 3

The focus here is the force density of the MLA. For this case the outer diameter of the MLA is constrained with the current outer dimensions of the MLA. Thus, it will be possible to find the optimal relation between the geometric parameters.

2. Description of Linear Actuators

The functionalities of the MeLA and MLA are elaborated in this section.

2.1 MeLA

The MeLA works with the nut and screw principle by using a gearing from the BLDC motor to the leadscrew, as illustrated in figure 1, where the grey areas symbolize geometry going out of the paper.

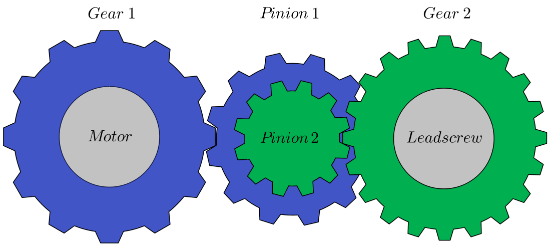

Fig. 1 Simplified working principle of the MeLA

According to the datasheet [1], the MeLA can actuate with a load of 6800 N and self-lock at loads of up to 8800 N. These are the primary specifications the MLA will be compared to. Additional relevant specifications are the volume and the geometric dimensions. The specifications are shown in table I.

Specification	Value
Dimensions	(500 + Stroke length) x 148 x 76 mm
Max. Load	6800 N
Self-lock	8800 N

Tab. I Specifications of the LA36

2.2 MLA

The MLA prototype is the main focus of this paper and will be elaborated more thoroughly than the MeLA. The MLA is seen in figure 2, and subsequently some terminology will be established.

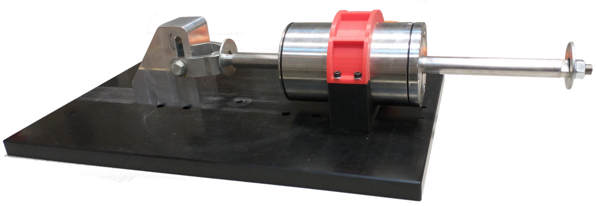

Fig. 2 The MLA on its baseplate

Terminology

A 3D CAD model of the MLA is utilized for illustration purposes. Figure 3 shows two different cross-sectional views of the MLA. The most significant components in regards to this paper are indicated with orange arrows.

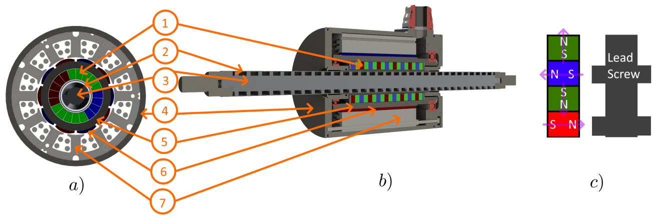

Fig. 3 Illustration for terminology

Lead Magnets	(1)	*Rotor*	(5)
Leadscrew Sleeve	(2)	*Rotor Magnets*	(6)
Leadscrew	(3)	*Stator*	(7)
Housing	(4)		

Translator

The translator refers to the leadscrew with sleeve. It is used to refer to the overall function of the part, which is moving linearly. When the word leadscrew is used, it is specifically referring to the leadscrew as a component without the sleeve.

Magnet Colors

Red magnet means north is inwards, blue means north is outwards, green refers to north pointing toward the adjacent red magnet. as illustrated to the far right in figure 3.

Mode of Operation

The MLA works by creating a reluctance force in the ferromagnetic leadscrew. Figure 4 shows a cross-section of the MLA innards, i.e. rotor and inwards, where the functioning of the leadscrew and magnetic nut is seen, although sleeves have been omitted for simplicity. The double helix leadscrew is surrounded by dozens of specially fabricated permanent magnets arranged specifically to create helices of magnets with the same lead as the leadscrew. The magnets are sintered NdFeB N45H with a remanent flux density of 1.32 - 1.38 T (1.35T mean) [2]. The magnets are furthermore arranged axially in a Halbach array [3] to maximize the magnetic flux on the side with the leadscrew. This is the reason behind the composition shown in figure 3 c).

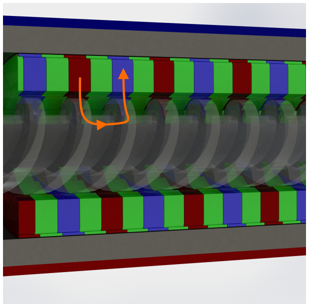

Fig. 4 MLA innards close up

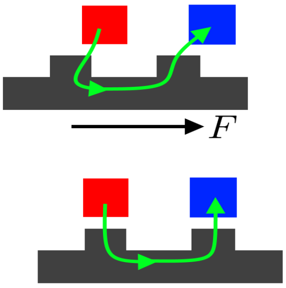

Fig. 5 Reluctance force

The flux will rather flow through the material with the highest permeability, which is the steel helix. When the steel helix is displaced axially from the magnets, the concentrated flux in the permeable material will cause reluctance forces that influences the material to align itself with the flux of the permanent magnets. This is indicated in figure 4 by the orange arrow symbolizing the flux. Figure 5 shows the principle in a simplified manner.

3. Magnetic Linear Actuator Experiments

Two separate experiments are carried out to determine the nature of the magnetic field and the stall force.

3.1 Stall Force

The stall force is defined as the maximum reluctance force, that the magnetic threads and leadscrew can provide. This occurs at a certain point during slip, i.e. axial displacement between lead magnets and translator threads.

The stall force is found by disassembling the MLA and fixating the rotor in a vice, as shown in figure 6. The figure also depicts the force transducer and positioning table used for force and displacement measurements. The positioning table is used to move the translator of the MLA in steps of $0.2\,\mathrm{mm}$.

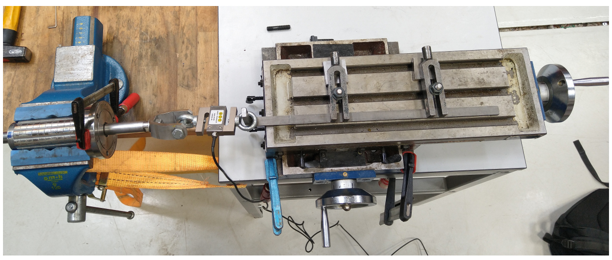

Fig. 6 Setup used during stall force experiments

The experiment is conducted thrice, to demonstrate repeatability. The results from the experiments can be seen on figure 7, along with the difference between each data point.

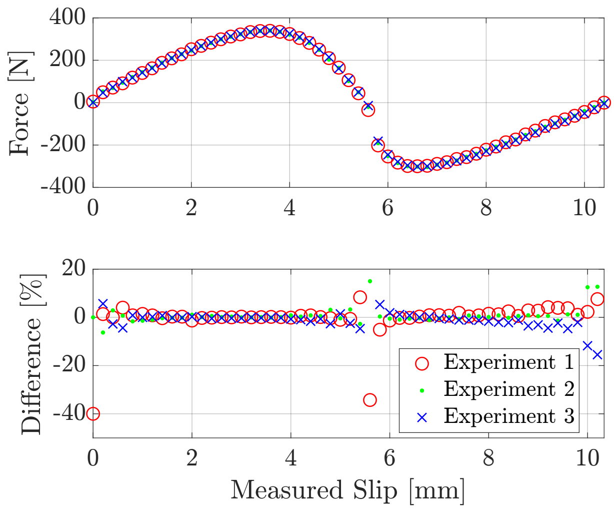

Fig. 7 Slip versus force. below: difference from mean

From the experiments the stall force is found to be $330\,\mathrm{N}$. Furthermore, the slip distance at the last data point is found to be $10.4\,\mathrm{mm}$. This is close to the pitch of the leadscrew, which is $11\,\mathrm{mm}$. This means that the setup contains $0.6\,\mathrm{mm}$ of play, which could be a contributing factor to the relatively sharp descent at the point where the force crosses zero.

3.2 Magnetic Field

The magnetic field of the inside of the rotor produced by the lead magnets is measured using a teslameter.

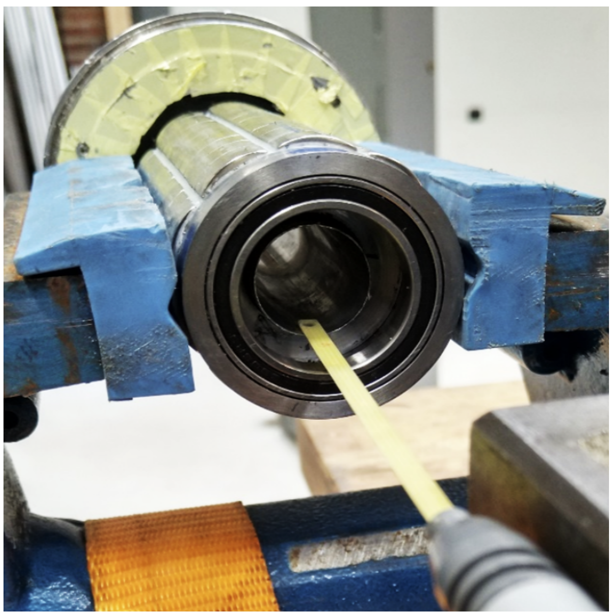

Fig. 8 Setup used to measure magnetic field

The flux is both measured along the rotor axis and the inner circumference of the rotor. The setup for flux measurements along the rotor axis is shown on figure 8. The teslameter is mounted on a positioning table, which is moved in steps of $0.4\,\mathrm{mm}$. To measure the magnetic field along the circumference, the rotor is mounted vertically and rotated in steps of $18\,°$, while keeping the teslameter stationary. The results of the measurements can be seen in figure 9.

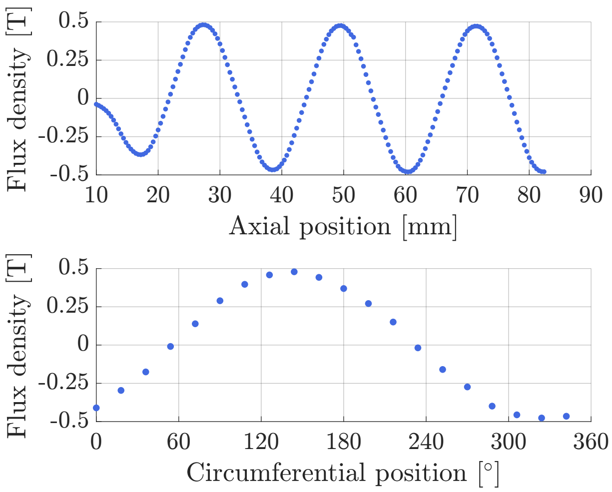

Fig. 9 Flux density measurements

These discrete measurements are extra- and interpolated to the entire rotor and can be seen below in figure 10. The figure depicts the magnetic field along the length and around the circumference, where the positional coordinates are mapped onto a 2D-plane.

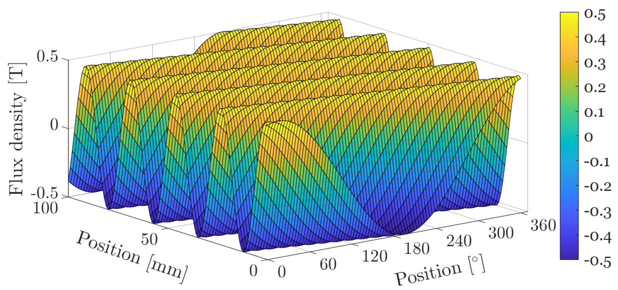

Fig. 10 Extra- and interpolated flux density inside the rotor

The experimental data correspond to what is expected from the CAD model of the MLA concerning lead, pitch and magnet arrangement. The data will furthermore be used in section 5 to validate the FE model of the MLA.

4. Design of Self-Lock

It is of interest to design a mechanism for self-lock, such that the MLA is locked when zero power is applied. It was noted from experiments, that the stall force with zero power (open-circuit) is only a third of the ordinary stall force. The self-lock force should mimic that of the MeLA which is 30% larger than its stall force. The self-lock force of the MLA must consequently be $430\,\mathrm{N}$.

4.1 Concept Generation Methods

The functionalities that must be achieved by the self-lock mechanism are:

- Stall Force of $430\,\mathrm{N}$ when powered off
- No Significant frictional wear for long lifetime
- Low volume
- Efficient locking i.e. small power losses
- Low Cost

Concepts are generated using both brainstorming and -writing methods which are evaluated in decision matrices, where the criteria are the weighted functionalities. [4]

4.2 Chosen Design

The chosen concept is a translator clamp as illustrated in figure 11 and 12. It utilizes a spring-actuator system, where the spring is preloaded to clamp the translator such that it is fixated when the MLA is powered off. The clamp is made of steel and will be located on the inside of the housing which needs to be expanded. To open the clamp, a solenoid linear actuator is used. This concept can provide a friction force larger than the stall force but does not hinder the MLA in any way during ordinary operation.

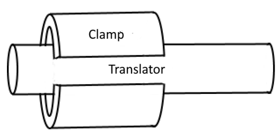

Fig. 11 Self-lock concept

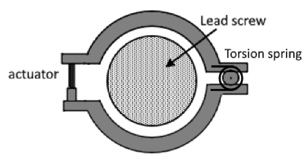

Fig. 12 Self-lock detailed

Spring and Actuator Scaling

The torsional spring must be chosen on basis of the required frictional force and is assumed to be linear. It is assumed that the distributed force on the translator from the clamp can be idealized as a resulting normal force as illustrated in figure 13.

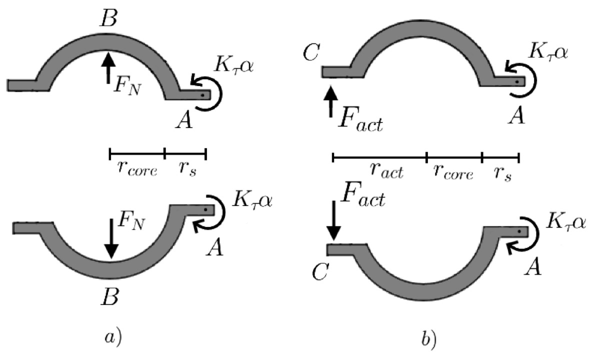

Fig. 13 FBD of clamp with torsional spring: *a)* Locked *b)* Open

The friction force μF_N must be 130% of the stall force $F_{stall} = 330\,\text{N}$, to comply with the specification of the MeLA. This yields a normal force of:

$$\mu F_N = 1.3 F_{stall} \Rightarrow F_N = \frac{1.3 F_{stall}}{\mu} = 703.3\,\text{N} \quad (1)$$

Here $\mu = 0.61$ is the static friction coefficient of aluminium on steel in contact [5]. The torsional spring is mounted a distance of $r_{core} + r_s = 25\,\text{mm}$ from the resulting normal force. The radius of the spring is based on the datasheet for the spring TO-5239 [6]. Hereby, the required moment can be found by moment equilibrium around point A as:

$$F_N \cdot 25\,\text{mm} = K_\tau \alpha = 17.6\,\text{Nm} \quad (2)$$

Here K_τ is the torsional spring coefficient and α is the angular displacement. A sufficient combination of spring coefficient and initial displacement is found to be $K_\tau = 88.392\,\frac{\text{Nmm}}{\text{deg}}$ with the spring TO-5239 and $\alpha = 199\,\text{deg}$ respectively.

The concept is deemed feasible for the current MLA, as the necessary self-lock force is provided.

5. Modelling

The magnetic field interaction between the lead magnets and the leadscrew is modelled using a finite element representation in COMSOL Multiphysics.

5.1 Finite Element Model

A 3D model as seen in figure 14 is most appropriate for the geometry and for modelling magnetic fields.

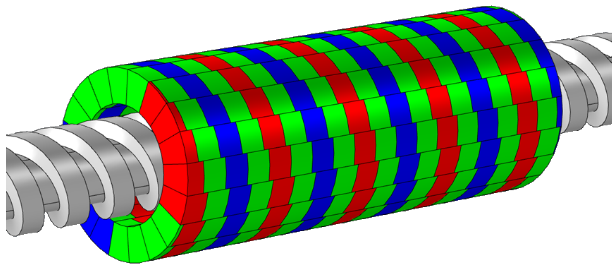

Fig. 14 3D model of the MLA

However, in order to reduce the computation time while yielding trustworthy results, a full-length 2D axisymmetric surrogate model is established and used in optimization. This model only includes the important elements, therefore disregarding sleeves, which are assumed to have a relative permeability of approximately 1. The geometric definitions can be seen in figure 15.

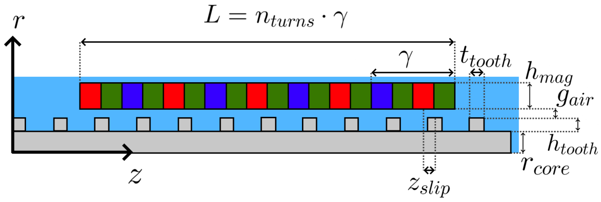

Fig. 15 2D axisymmetric model of the MLA

The initial values for these parameters are stated in table II.

Symbol	Initial Value	Description
γ	22 mm	Lead
r_{core}	6.18 mm	Radius of rod core
h_{tooth}	3.32 mm	Radial height of tooth
t_{tooth}	3.6 mm	Axial thickness of tooth
g_{air}	2.32 mm	Radial air gap
h_{mag}	7 mm	Radial height of magnets
z_{slip}	0 mm	Axial Slip
n_{turns}	4.5	Number of Turns

Tab. II Initial geometric parameters

5.2 Model Validation

To validate the finite element model, the measured slip versus force is compared to parameter sweeps in COMSOL, where the slip is increased in steps, from 0 to 11 mm. This is done for both the 2D and 3D model. The parameter sweeps are superimposed on the data from figure 7, which results in figure 16.

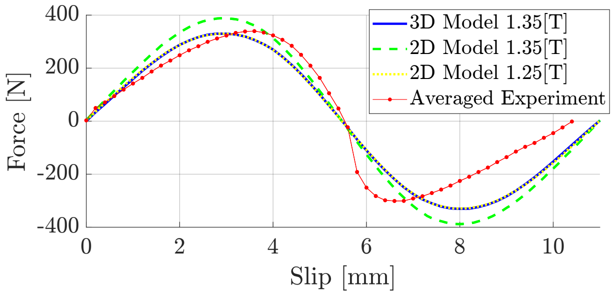

Fig. 16 Comparison of experimental and simulated slip versus force

It is evident from the figure that the 3D model and the 2D model differ slightly from the experiments. However, the 3D model resembles the experiments more accurately. It can also be seen that if the remanent flux density of the magnets in the 2D model is reduced to $1.25\,\mathrm{T}$, it results in a curve much closer to the 3D model. Reducing the remanent flux density in the 2D model leads to a less accurate representation of the magnetic field inside the magnets, which yields more accurate results for the flux in the air gap between magnets and leadscrew, which is more important for the accuracy of the reluctance force.

A comparison is made of the experimentally found magnetic field to multiple simulated magnetic fields. The z-position on figure 17, uses the same coordinate system as that of figure 15.

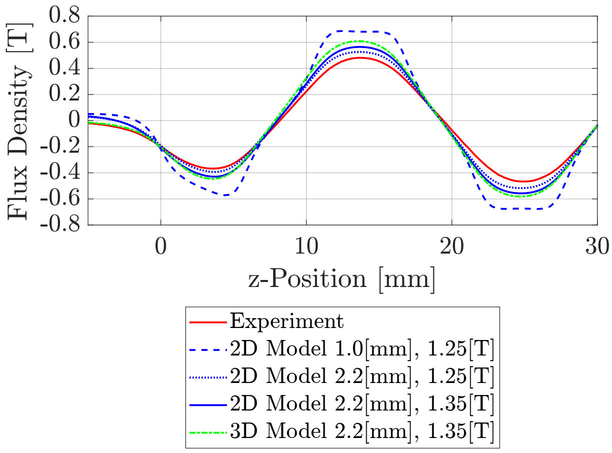

Fig. 17 Comparison of magnetic fields

In figure 17, both the distance from the magnet to where the magnetic field is measured and the remanent flux density of the magnet is given. During the flux experiment, the teslameter is at a distance of $\approx 2\,\mathrm{mm}$ from the magnets, because of various sleeves and air gaps. From the figure, it is seen that both of the simulations where the remanent flux density is set to $1.35\,\mathrm{T}$, overestimate the flux density. Using $1.25\,\mathrm{T}$ combined with the 2D model gives a curve closer to that of the experiments. A simulation is also made, where the flux is measured at a distance of $1\,\mathrm{mm}$ from the magnet. Here the saturation is visible.

On the basis of both validations, the 2D model with magnets that have a remanent flux density of $1.25\,\mathrm{T}$ is used during optimization, since it models the reluctance force with appropriate fidelity.

6. Optimization

To perform the optimization, MATLAB's fmincon function is used [7], where it is specified to utilize a SQP algorithm which estimates the hessian based on the finite different gradients calculated in a MATLAB function with data from COMSOL evaluations of the stall force [8]. Three separate optimization cases are investigated. The design variables for the optimization are shown below in equation 3.

$$\boldsymbol{x} = [n_{turns} \quad h_{magnet} \quad h_{tooth} \quad r_{core} \quad \gamma \quad t_{tooth}]^T \tag{3}$$

For each case, the objective functions with constraints are stated. All cases are subject to the following upper and lower bounds shown in equations 4 and 5.

$$\boldsymbol{ub} = [100 \quad 1\mathrm{m} \quad 1\mathrm{m} \quad 1\mathrm{m} \quad 0.1\mathrm{m} \quad 1\mathrm{m}]^T \tag{4}$$

$$\boldsymbol{lb} = [1 \quad 1\mathrm{mm} \quad 1\mathrm{mm} \quad 1\mathrm{mm} \quad 5\mathrm{mm} \quad 1\mathrm{mm}]^T \tag{5}$$

6.1 Case 1

The objective function for case 1 is seen in equation 6

$$Minimize: \quad \mathcal{F}_1(\boldsymbol{x}) = -\Psi F(\boldsymbol{x}) \tag{6}$$

where Ψ is an objective function scaling factor and F is the simulated force. The objective function is subject to the linear inequality constraint shown in equation 7. The linear constraint, limits the maximum permissible outer radius of the optimized MLA. The maximum radius is based on the dimensions of the MeLA.

$$[0 \quad 1 \quad 1 \quad 1 \quad 0 \quad 0]\,\boldsymbol{x} \leq 0.042 \tag{7}$$

The nonlinear inequality constraints are established to constrain both the length of the MLA and the geometric ratios for manufacturing and computational purposes.

The nonlinear constraints for case 1 can be seen in equation 8.

$$\boldsymbol{c}_1(\boldsymbol{x}) = \begin{bmatrix} 2\cdot n_{turns}\cdot\gamma - 1 \\ \frac{h_{tooth}}{2\cdot r_{core}} - 1 \\ -(10\cdot\frac{h_{tooth}}{r_{core}} - 1) \\ \frac{1}{0.95}\cdot 2\cdot\frac{t_{tooth}}{\gamma} - 1 \\ -(100\cdot 2\cdot\frac{t_{tooth}}{\gamma} - 1) \\ \frac{0.8\cdot h_{magnet}}{\gamma} - 1 \end{bmatrix} \leq \boldsymbol{0} \qquad (8)$$

6.2 Case 2

The objective function for case 2 is a least square formulation seen in equation 9.

$$Minimize: \quad \mathcal{F}_2(\boldsymbol{x}) = \Psi[(F_L - F(\boldsymbol{x}))^2 + WV(\boldsymbol{x})] \qquad (9)$$

With this formulation, the squared term which is the force error will be the smallest i.e. zero when the two forces are equal. Meanwhile the weighted volume expression $WV(\boldsymbol{x})$ must also be lowered. This means that the algorithm ideally will try to minimize the volume even if the force is already optimized.

The objective function is not subject to any linear constraints. It is however subject to the same nonlinear constraints as for case 1, shown in equation 8. The first nonlinear constraint is not included since it limits the length.

6.3 Case 3

The objective function for case 3 is seen in equation 10.

$$Minimize: \quad \mathcal{F}_3(\boldsymbol{x}) = -\Psi\frac{F(\boldsymbol{x})}{V(\boldsymbol{x})} \qquad (10)$$

The objective function is subject to the linear constraint shown in equation 11. The linear constraint limits the maximum permissible outer radius of the optimized MLA to the outer radius of the current MLA.

$$[0 \quad 1 \quad 1 \quad 1 \quad 0 \quad 0]\,\boldsymbol{x} \leq 0.0165 \qquad (11)$$

Additionally case 3 is subject to a modified version of the nonlinear constraints, where the first constraint is slightly modified, as shown in equation 12

$$\boldsymbol{c}_3(\boldsymbol{x}) = \begin{bmatrix} 10\cdot n_{turns}\cdot\gamma - 1 \\ \frac{h_{tooth}}{2\cdot r_{core}} - 1 \\ -(10\cdot\frac{h_{tooth}}{r_{core}} - 1) \\ \frac{1}{0.95}\cdot 2\cdot\frac{t_{tooth}}{\gamma} - 1 \\ -(100\cdot 2\cdot\frac{t_{tooth}}{\gamma} - 1) \\ \frac{0.8\cdot h_{magnet}}{\gamma} - 1 \end{bmatrix} \leq \boldsymbol{0} \qquad (12)$$

7. Results

7.1 Case 1

The objective function is scaled with a factor of $\frac{1}{33}$, as a result of a normalization and consideration of the gradients of the design variables. The optimization can be seen iteration by iteration in figure 18.

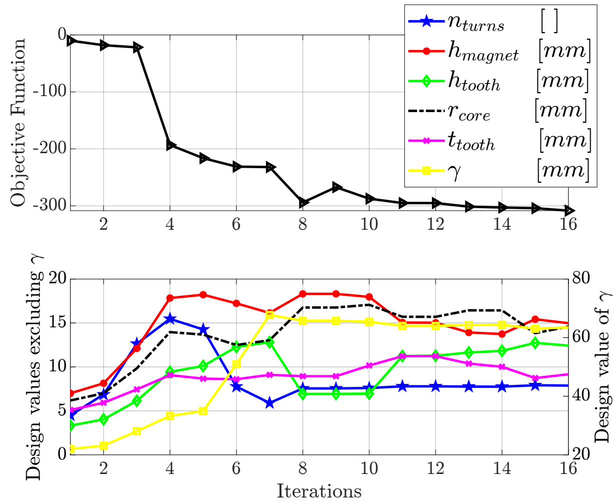

Fig. 18 Evolution of design variables and objective function

The optimization reaches a maximum stall force of 10.2 kN, within the geometrical constraints. This force is approximately 50% larger than the stall force of the MeLA. The force density reaches 1089 $\frac{\mathrm{N}}{\mathrm{L}}$. The optimized MLA design for this case is seen in figure 19 and 20 which displays the full model and a zoom-in on a single lead respectively. Here it is possible to see the direction and density of the flux travelling within the leadscrew from the magnets.

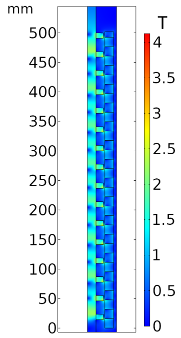

Fig. 19 Case 1: full model

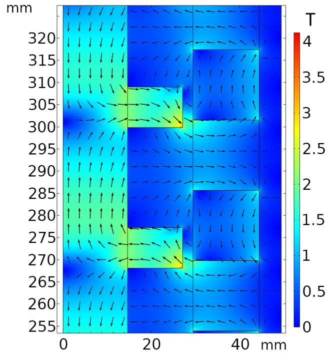

Fig. 20 Case 1: zoom view

7.2 Case 2

The objective function utilizes a weight factor of $W = 10^{-7}$ on the volume expression and a scaling factor of 10 on the objective function as a result of normalization and based upon the design variable gradients. These are determined through an iterative process and yield the results seen in figure 21.

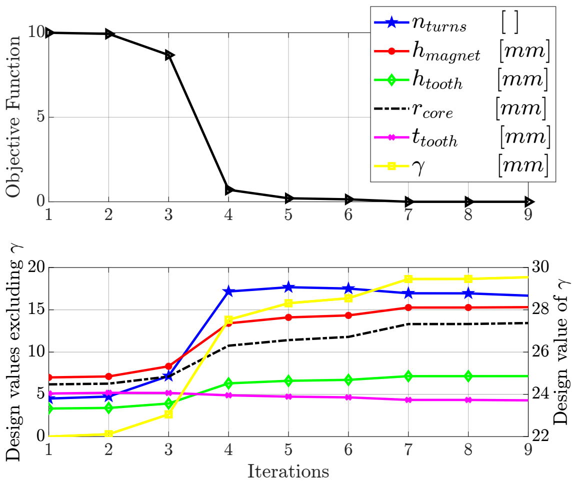

Fig. 21 Evolution of design variables and objective function

Case 2 reaches a maximum stall force at 6797 N, which is within 3 N of the stall force of the MeLA. The force density reaches 876.15 $\frac{\mathrm{N}}{\mathrm{L}}$.

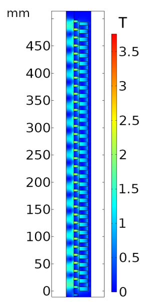

Fig. 22 Case 2: full model

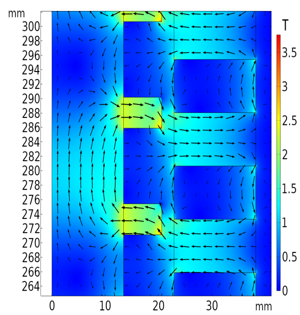

Fig. 23 Case 2: zoom view

The optimized design for case 2 is seen in figure 22 and 23.

7.3 Case 3

During the optimization of case 3, it is found that using the objective function shown in equation 10, does not yield usable results. The optimization does not go far from its initial design point and achieves only a negligible increase in force, even for different scaling. The objective function from case 1 is therefore used, with a scaling of 10^{-4}, which gives the results shown in figure 24. This assumes that the optimization utilizes the maximum allowable radius the initial design values, which should make the volume change insignificant.

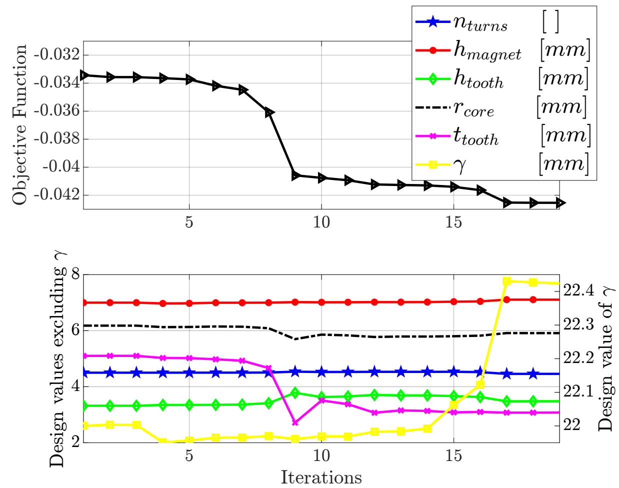

Fig. 24 Evolution of design variables and objective function

The optimization reaches a stall force of 425.40 N, within the geometrical constraints of the original MLA. The force density reaches 402.84 $\frac{\mathrm{N}}{\mathrm{L}}$.

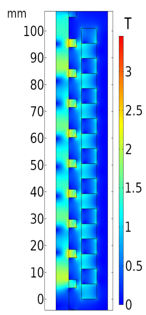

Fig. 25 Case 3: full model

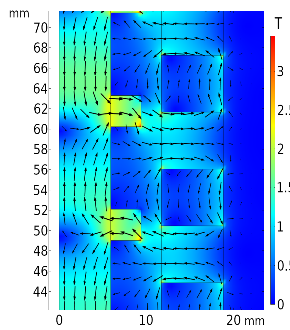

Fig. 26 Case 3: zoom view

Figure 25 and 26 displays the optimized model including its length, flux direction and density.

8. Discussion

The case results of the optimizations will be discussed along with the process behind the final results.

8.1 Case 1

For case 1 the initial objective function yielded an unusual result, which did not converge. By adding a scaling factor the optimization was able to keep going past the 4^{th} iteration and converge on the 16^{th} iteration. The optimization reaches a stall force of $10.2\,\mathrm{kN}$, which is above the stall force of the MeLA. Regarding the constraints, the radius is at the limit and the length is $0.0091\,\mathrm{mm}$ from the limit, which means that the optimization is utilizing all the allowable volume. This gives a rather high force density of $1089.48\,\frac{\mathrm{N}}{\mathrm{L}}$. This means that the MLA potentially can replace the MeLA. However, the constraints for case 1 were meant to mimic the dimensions of the MeLA, but since the MeLA is not cylindrical, the comparison is not exactly fair. The optimum redesign of the MLA reaches a larger volume than that of the MeLA.

8.2 Case 2

For case 2 the objective function without any scaling became computationally expensive and had convergence problems, as the gradients became too small due to the normalization which resulted in an increase of evaluations. The volume weight factor used was found through several iterations and is therefore undoubtedly not the optimum weight factor for this case. The scheme yields results which achieve the objective of the optimization, as it reaches a stall force that is within $\approx 0.05\%$ of the $6800\,\mathrm{N}$. The weight factor used is the one that yields the highest force density of the ones tested through the iterative process. A raise of the weight factor appears to be the obvious choice when an increase in the force density is desired but causes the error between the forces to increase undesirably.

8.3 Case 3

For case 3, it is difficult to get the optimization to make radical changes to the initial design. No difference in the optimization is noted when using a simple expression for the volume of the MLA instead of a complex expression where the air inside the MLA is not included. When the volume is removed from the objective function, it gave a noticeable result when the scaling is set to 10^{-4}. The optimum redesign for case 3 results in a stall force of $425.40\,\mathrm{N}$ with a force density for the redesigned MLA of $402.84\,\frac{\mathrm{N}}{\mathrm{L}}$

It should be noted that when the volume is removed from the objective function, the optimization problem resembles that of case 1. The only difference is the volume constraint. Case 1 is limited by the dimensions of the MeLA, while case 3 is limited by the dimensions of the current MLA.

8.4 Final Comparison

In table III the initial and final design variables of the optimized MLAs are shown. Furthermore, the force density is included. It is evident that case 1 has more than three times the original force density. This is done by increasing the stall force thirtyfold whilst only increasing the volume tenfold. Case 2 more than doubles the force density while having the wanted stall force of $\approx$6800 N. Considering that the final design of case 3 utilizes the same space as the original, and increases the stall force by 26%, the optimization seems to have improved the design favourably.

	MeLA	**MLA**	**Case 1**	**Case 2**	**Case 3**	*Unit*
n_{turns}	n/a	4.5	7.88	16.7	4.46	
h_{magnet}	n/a	7	15.0	15.3	7.12	*mm*
h_{tooth}	n/a	3.32	12.4	7.16	3.48	*mm*
r_{core}	n/a	6.18	14.6	13.4	5.91	*mm*
γ	n/a	22	63.5	29.5	22.4	$\frac{mm}{rev}$
t_{tooth}	n/a	5.1	9.16	4.29	3.08	*mm*
z_{slip}	n/a	2.9	10.8	3.69	2.98	*mm*
F	6.8	0.334	10.2	6.80	0.425	*kN*
V	3.05	1.05	9.34	7.76	1.06	*L*
F/V	2230	319	1090	876	403	$\frac{N}{L}$

Tab. III Comparison of rounded design values for different MLAs and for the MeLA

8.5 Optimal Geometric Ratios

An interesting aspect of the optimizations is also the geometric ratios, which potentially can be helpful when designing a MLA. For the three optimization cases and the original design the ratios are shown in table IV.

	$\frac{h_{tooth}}{t_{tooth}}$	$\frac{h_{tooth}}{r_{core}}$	$\frac{t_{tooth}}{\gamma/4}$	$\frac{n_{turns}}{\gamma}$
Initial	0.651	0.537	0.927	0.205
Case 1	1.357	0.852	0.577	0.124
Case 2	1.669	0.533	0.581	0.564
Case 3	1.130	0.589	0.549	0.199

Tab. IV Geometric ratios

The ratios are different for each case, which means that if it is desired to design a MLA of a certain size, it is not sufficient in regards to optimum design to simply scale the geometry with constant factors. The ratios of all three cases agree upon whether the optimized ratios should be less or larger than 1 in contrast to the initial design.

9. Conclusion

The conclusion treats the results and findings of the investigation of optimum redesign of the MLA

To accomplish this investigation, three cases were established, which treat different purposes leading to different optimum redesigns.
The purpose of case 1 was to redesign the MLA such that it achieved the largest possible stall force while being constrained by the geometric dimensions of the MeLA. This lead to a redesign with a stall force of $10.2\,\mathrm{kN}$ and the highest force density of $1090\,\frac{\mathrm{N}}{\mathrm{L}}$ which is $\approx 50\%$ of the force density of the MeLA.
The purpose of case 2 was to match the force of the MeLA, but without the geometric dimension constraints. This resulted in a stall force of $6.78\,\mathrm{kN}$ with a force density of $876\,\frac{\mathrm{N}}{\mathrm{L}}$.
The purpose of case 3 was to optimize the force density of the MLA within the boundaries of the current MLA. This resulted in an increase of the stall force by 26.4% to $425.4\,\mathrm{N}$. However during optimization of case 3 the force density objective function does not yield usable results, and an optimization regarding force was therefore used instead.

Comparing the original design and redesigns showed that all of the cases improve the force density compared to the original design. It is therefore concluded that all of the three redesigns are improvements from the original design, which was the focus of this project. It is also concluded that a reluctance-based MLA can replace a MeLA in terms of stall force.

It is concluded that the findings made throughout the cases tend towards the optimum MLA ratios when aiming towards a high force density. The mean optimum ratios are seen in the following table V.

	$\frac{h_{tooth}}{t_{tooth}}$	$\frac{h_{tooth}}{r_{core}}$	$\frac{t_{tooth}}{\gamma/4}$	$\frac{n_{turns}}{\gamma}$
Mean optimum values	1.39	0.66	0.570	0.23

Tab. V Optimum MLA ratios

Is is concluded that the self-lock design is able to lock the MLA which can withstand a load up to 30% higher than the stall force. However more research is necessary to determine whether it is a feasible solution for a larger redesigns of the MLA.

Acknowledgement
The authors of this work gratefully acknowledge Grundfos for sponsoring the 10$^{\text{th}}$ MechMan symposium.

References

[1] Linak, “Ln 36 datasheet,” 2022.
[2] Arnold Magnetic Technologies Corp., Sintered Neodymium-Iron-Boron Magnets, 2017.
[3] S. M. J.E. Hilton, “An adjustable linear halbach array,” Journal of Magnetism and Magnetic Materials, 2012.
[4] D. G. Ullman, The Mechanical Design Process. 621 Aeronca St. Independence Oregon 97351: David G. Ullman, 2018.
[5] R. L. Norton, Machine Design - An Integrated Approach. Pearson, 5$^{\text{th}}$ ed., 2014.
[6] MWcomponents, “Spring to-5239,” 2022.
[7] MathWorks, “fmincon,” 2022.
[8] J. Arora, Introduction to Optimum Design. Elsevier Science Publishing Co Inc, 2016.